# Femtosecond laser heating of multi-layer metals—I. Analysis

**Article** *in* International Journal of Heat and Mass Transfer · November 1994

DOI: 10.1016/0017-9310(94)90396-4

Pergamon

*Int. J. Heat Mass Transfer.* Vol. 37, No. 17, pp. 2789–2797, 1994

0017–9310/94 $7.00+0.00

0017–9310(94)E0050–5

# Femtosecond laser heating of multi-layer metals—I. Analysis

T. Q. QIU and C. L. TIEN†

Department of Mechanical Engineering, University of California, Berkeley, CA 94720, U.S.A.

(*Received* 2 *February* 1993)

**Abstract**—Multi-layer metal films such as metallic coatings on metal substrate are important elements in modern engineering applications. Specifically, gold-coated metal mirrors are widely used in high-power laser systems. This work studies microscopic energy deposition and transport processes during short-pulse laser heating of multi-layer metals: the absorption of radiation energy by free electrons and the energy exchange between electrons and the lattice. The results show that multi-layer metals present very different thermal responses from single-layer metals during the heating process. In a gold and chromium multi-layer film, although laser energy is absorbed by free electrons in the top gold coating layer, most of the absorbed energy is converted into lattice energy not in the gold layer but rather in the underlying chromium layer. The underlying chromium layer reduces the lattice-temperature rise of the top gold layer significantly during short-pulse laser heating, suggesting a new way to increase the resistance of mirrors to thermal damage in applications of high-power lasers.

## INTRODUCTION

MULTI-LAYER metal thin-films are widely used in engineering applications since a single metal layer often cannot satisfy all mechanical, thermal and electronic requirements. A better understanding of energy transfer in such multi-layer systems is critical in many applications. For example, high-power infrared-laser systems often use gold-coated metal mirrors because of their extremely high reflectivity—typically over 97%. Even with such high reflectivity, a small but significant portion of laser energy is still absorbed in the coatings, which can cause excessive heating and thermal damage to the mirrors.

Conventionally, the thermal design of mirrors is based on the Fourier heat conduction model [1, 2]. As predicted from the Fourier model, materials with a higher thermal diffusivity spread heat faster, which in turn reduces the risk of thermal damage. Therefore, the thermal diffusivity is often considered the most important thermal parameter in choosing coating and substrate materials [3]. This design concept is valid for systems with relatively long laser pulses. But, for high-power and short-pulse lasers, this concept is subject to question since its physical basis the Fourier heat conduction model—might not be valid in the short time-scale. For example, non-Fourier heat conduction has long been considered [4–8] and observed in many materials at cryogenic temperatures [9–13].

Laser heating of metals involves two major microscopic energy deposition processes: absorption of radiation energy by free electrons and subsequent heating of the metal lattice through electron–lattice collisions. Kaganov *et al.* [14] predicted a finite rate of energy exchange between electrons and the lattice. Anisimov *et al.* [15] proposed a phenomenological model to describe effects of the electron–lattice energy exchange on laser heating of metals. They predicted that free electrons can be heated to a temperature much higher than the lattice temperature during high-power laser heating. Such electron–lattice non-equilibrium heating processes have been observed recently in many single-layer metals [16–20]. The non-equilibrium laser-heating processes result in a totally different thermal response of the metal lattice compared to predictions from the conventional Fourier conduction model [15, 21]. Non-equilibrium laser heating of multi-layer metals, however, has not been studied.

The purpose of this work is to investigate energy transfer in multi-layer metals during short-pulse laser heating. The present paper (Part I) and the following paper (Part II) will focus on theoretical and experimental studies, respectively. The major effort is to investigate effects of underlying metals on the thermal response of the top coating layer. This study also addresses the necessary introduction of an additional parameter besides the thermal diffusivity—the electron–lattice coupling factor—to characterize thermal properties of coatings and substrates in the thermal design of mirrors.

† Author to whom correspondence should be addressed.

## NOMENCLATURE

| | |
|---|---|
| $C$ | heat capacity [J m$^{-3}$ K$^{-1}$] |
| $G$ | electron–lattice coupling factor [W m$^{-3}$ K$^{-1}$] |
| $J$ | laser pulse intensity [J m$^{-2}$] |
| $k$ | Boltzmann constant [J K$^{-1}$] |
| $L$ | film thickness [m] |
| $m$ | effective mass of electrons [kg] |
| $n$ | electron number density [m$^{-3}$] |
| $\mathbf{Q}$ | heat flux [W m$^{-2}$] |
| $R$ | surface reflectivity |
| $S$ | source term [W m$^{-3}$] |
| $t$ | time [s] |
| $t_c$ | electron–lattice thermalization time, $t_c = C_{e0}/G$ [s] |
| $t_h$ | characteristic laser heating time [s] |
| $t_p$ | laser pulse duration [s] |
| $T$ | temperature [K] |
| $x$ | spatial coordinate [m]. |

Greek symbols

| | |
|---|---|
| $\delta$ | radiation penetration depth [m] |
| $\kappa$ | thermal conductivity [W m$^{-1}$ K$^{-1}$] |
| $\tau$ | electron relaxation time [s]. |

Subscripts

| | |
|---|---|
| 0 | reference temperature |
| e | electron |
| eq | equilibrium |
| $\ell$ | lattice. |

## LASER HEATING MECHANISMS

Laser heating of metals is commonly described by the Fourier heat conduction model as:

$$C\frac{\partial T}{\partial t} = \nabla\cdot(\kappa\nabla T) + S, \tag{1}$$

where $C$ is the volumetric heat capacity, $\kappa$ is the thermal conductivity, and $S$ is the laser heating source term. The Fourier model can be called the parabolic one-step radiation model (POS) due to its two major assumptions. First, radiation energy is assumed to be converted into lattice energy instantaneously. Second, energy transfer in solids is assumed to be a diffusion process.

During short-pulse laser heating, these basic assumptions of the POS model are subject to question. For example, wave-type propagation of heat, instead of diffusion, has been proposed [4, 22], which results in the hyperbolic one-step radiation heating model (HOS):

$$C\frac{\partial T}{\partial t} = -\nabla\cdot\mathbf{Q} + S, \tag{2}$$

$$\tau\frac{\partial \mathbf{Q}}{\partial t} + \kappa\nabla T + \mathbf{Q} = 0, \tag{3}$$

where $\mathbf{Q}$ is the heat flux and $\tau$ is the relaxation time of free electrons in a metal.

Anisimov *et al.* [15] proposed that the conversion of radiation energy into internal energy is not instantaneous but involves two energy-deposition steps: (1) radiation heating of free electrons; and (2) the subsequent energy redistribution between electrons and the metal lattice. By further assuming that the electron and the lattice sub-systems can be characterized by an electron temperature, $T_e$, and a lattice temperature, $T_\ell$, respectively, they proposed a parabolic two-step radiation heating model (PTS):

$$C_e(T_e)\frac{\partial T_e}{\partial t} = \nabla\cdot(\kappa\nabla T_e) - G(T_e - T_\ell) + S, \tag{4}$$

$$C_\ell(T_\ell)\frac{\partial T_\ell}{\partial t} = G(T_e - T_\ell), \tag{5}$$

where $C_e$ and $C_\ell$ are the electron heat capacity and the lattice heat capacity, respectively, and $G$ is the electron–lattice coupling factor.

Fann *et al.* [23, 24] studied the validity of using an electron temperature to characterize the electron subsystem. By comparing the measured electron distribution functions with those predicted from equilibrium thermodynamics, the electron temperature is found to be well defined after the initial few hundred femtoseconds of laser heating. In the first few hundred femtoseconds, the use of the electron temperature is only approximate.

Qiu and Tien [25] removed the assumptions regarding instantaneous radiation deposition and diffusive energy transport in the POS model and derived a hyperbolic two-step model (HTS) rigorously from the Boltzmann transport equation for electrons:

$$C_e(T_e)\frac{\partial T_e}{\partial t} = -\nabla\cdot\mathbf{Q} - G(T_e - T_\ell) + S, \tag{6}$$

$$C_\ell(T_\ell)\frac{\partial T_\ell}{\partial t} = G(T_e - T_\ell), \tag{7}$$

$$\tau\frac{\partial \mathbf{Q}}{\partial t} + \frac{T_e}{T_\ell}\kappa\nabla T_e + \mathbf{Q} = 0. \tag{8}$$

Figure 1 summarizes the interrelationship between laser heating models based on three characteristic times during laser heating: (1) the characteristic heating time, $t_h$, which is either the laser pulse duration or the time needed to heat a material to a certain temperature; (2) the electron relaxation time, $\tau$; and (3) the electron–lattice thermalization time, $t_c = C_e/G$,

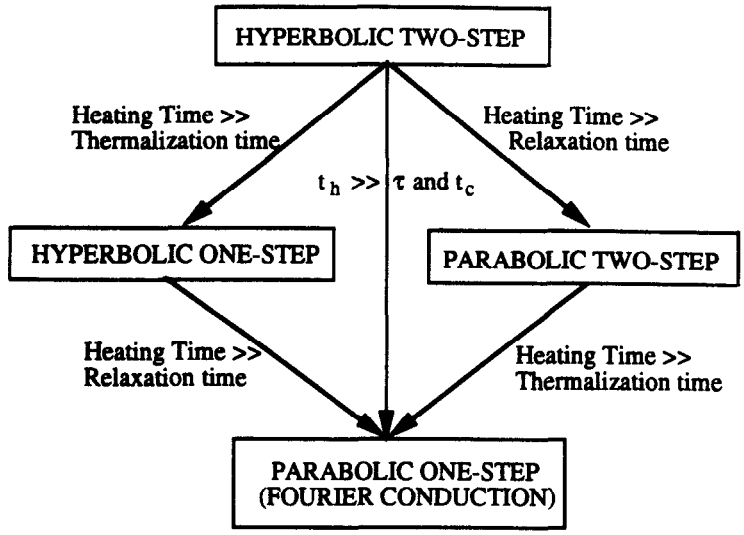


FIG. 1. Interrelationship between laser heating models

which is the time needed for electrons and the lattice to reach thermal equilibrium.

## LASER HEATING OF MULTI-LAYER METALS

Figure 2 shows a schematic diagram for laser heating of multi-layer metal films. Three film structures are studied in this paper, including gold single-layer, gold–chromium double-layer, and gold–chromium–gold triple-layer films. The total film thickness is 1000 Å in each case. Gold is chosen as the top layer due to its wide usage in mirror coatings, and chromium is chosen as the underlying layer because of its strong electron–lattice coupling and short electron–lattice thermalization time [26].

The electron–lattice thermalization time and the electron relaxation time determine energy transfer mechanisms during laser heating: whether energy deposition is a one-step process or a two-step process, and whether energy propagation is parabolic or hyperbolic. Figure 3 shows the thermalization time and relaxation time of noble metals from 10 K to 800 K. The thermalization time is taken from measurements [27] and the relaxation time is estimated from its relation to the thermal conductivity [28]:

$$\tau(T) = \frac{3m}{\pi^2 nk^2 T}\kappa(T), \tag{9}$$

where $n$ and $m$ are the number density and effective mass of free electrons, respectively, and $k$ is the Boltzmann constant. The thermal conductivity data are from Powell and Ho [29] and the other physical constants are from Kittel [28]. The thermalization time depends on temperature very weakly, but the electron relaxation time is extremely sensitive to the lattice temperature, especially at low temperatures. It increases dramatically as the temperature decreases, e.g. from 0.04 ps at room temperature to about 10 ps at 10 K. At high temperatures, the thermalization time

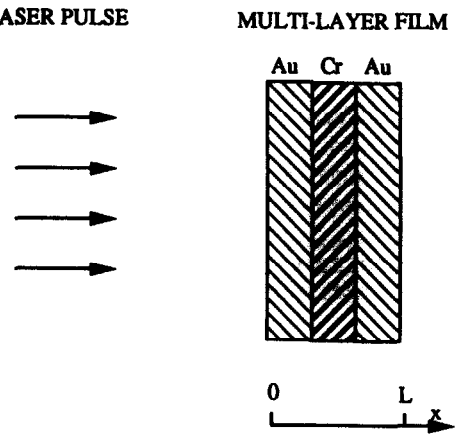


FIG. 2. Schematic diagram for laser heating of multi-layer metal films.

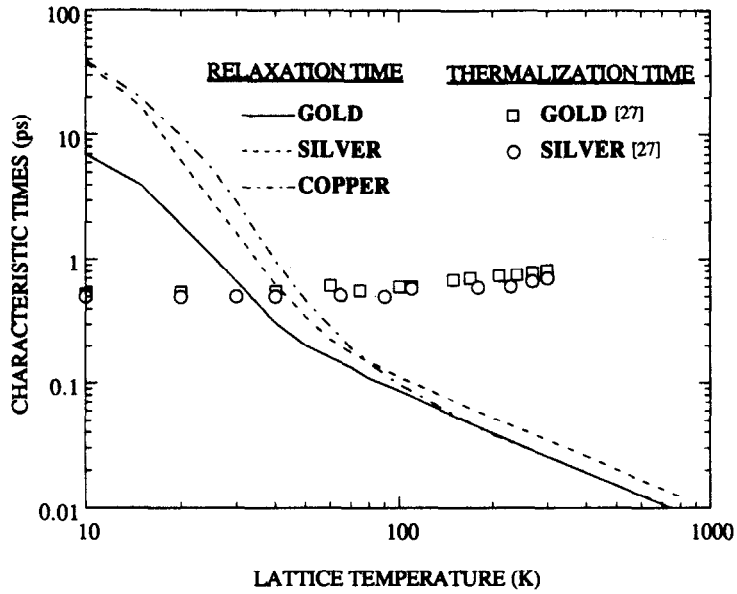


FIG. 3. Relaxation time and thermalization time of noble metals.

is longer than the relaxation time, indicating that the effect of two-step non-equilibrium heating is stronger than that of hyperbolic transport. At low temperatures the situation is reversed.

Figure 4 presents application regimes of laser heating models for gold. The onset of non-equilibrium laser heating and hyperbolic energy transport is chosen as $t_h = 5t_c$ and $t_h = 5\tau$, respectively. The POS model applies for slow heating processes, the PTS model applies for fast heating processes at relatively high temperatures, and the HOS model applies for low-temperature and fast heating processes. In certain low-temperature and fast heating regimes, the HTS model must be used.

This work considers short-pulse laser heating at room temperature and the case that the laser beam diameter is much larger than the heat penetration depth. Therefore, the heating process can be described by the one-dimensional PTS model as simplified from the HTS model:

$$C_e(T_e)\frac{\partial T_e}{\partial t} = \frac{\partial}{\partial x}\left(\frac{T_e}{T_\ell}\kappa\frac{\partial T_e}{\partial x}\right) - G(T_e - T_\ell) + S, \quad (10)$$

$$C_\ell\frac{\partial T_\ell}{\partial t} = G(T_e - T_\ell), \quad (11)$$

where the electron heat capacity is proportional to the

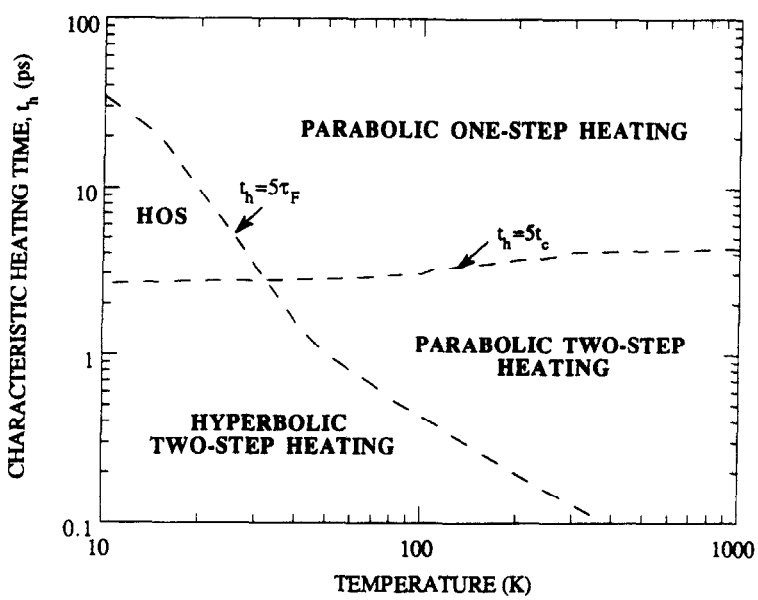


FIG. 4. Application regimes of laser heating models for gold.

electron temperature, and the thermal conductivity is modified by the ratio of the electron temperature and the lattice temperature. Equation (10) describes the change of the electron energy as a result of heat diffusion, energy exchange between electrons and the lattice, and radiation absorption. Equation (11) describes heating of the lattice through electron–lattice coupling. In pure metals, energy transport by free electrons is much greater than that by lattice vibrations. Therefore, heat diffusion by the lattice is neglected.

The spatial distribution of laser intensity is assumed to be uniform, and the temporal shape of the laser pulse is assumed to be Gaussian. By further neglecting the temperature dependence of optical properties [30, 31], the laser heating source term in equation (10) is:

$$S = 0.94\frac{1-R}{t_p\delta}J\cdot\exp\left[-\frac{x}{\delta}-2.77\left(\frac{t}{t_p}\right)^2\right], \quad (12)$$

where $R$ is the reflectivity, $\delta$ is the radiation penetration depth, $J$ is the total energy carried by a laser pulse divided by the laser spot cross section, $t_p$ is the full-width-at-half-maximum (FWHM) duration of the laser pulse, and time $t = 0$ is defined at the moment when the peak of a laser pulse arrives at the metal surface.

The initial conditions for both the electron and the lattice systems are:

$$T_e(x, -2t_p) = T_\ell(x, -2t_p) = T_0. \quad (13)$$

During the short period of laser heating, heat losses from the front and back surfaces of the film can be neglected, leading to the thermal-insulation boundary conditions,

$$\left.\frac{\partial T_e}{\partial x}\right|_{x=0} = \left.\frac{\partial T_e}{\partial x}\right|_{x=L} = \left.\frac{\partial T_\ell}{\partial x}\right|_{x=0} = \left.\frac{\partial T_\ell}{\partial x}\right|_{x=L} = 0. \quad (14)$$

At the gold–chromium interface, both the electron heat flux and temperature are continuous:

$$\left(\frac{T_e}{T_\ell}\kappa\frac{\partial T_e}{\partial x}\right)\Bigg|_{Au} = \left(\frac{T_e}{T_\ell}\kappa\frac{\partial T_e}{\partial x}\right)\Bigg|_{Cr} \quad T_e|_{Au} = T_e|_{Cr}. \quad (15)$$

Analytical solutions to the above equation are quite intractable due to the strong non-linearity of equation (10). The semi-implicit Crank–Nicholson scheme is therefore employed to solve the equations numerically. The electron and lattice temperatures are iterated for each time step until the convergence criteria are satisfied ($\Delta T_e/T_{e0} < 10^{-4}$ and $\Delta T_\ell/T_{\ell 0} < 10^{-5}$). A uniform grid system is used with 400 grid points. The total increase of the electron energy and lattice energy is calculated at certain times and compared with the absorbed radiation energy. The difference is within 0.1%. Furthermore, different grid spacing and time steps are used to check the consistency and stability of the numerical solutions. Material properties of gold and chromium used in the simulation are listed in Table 1.

## RESULTS AND DISCUSSION

Figure 5 shows the transient temperature profiles in a 1000 Å thick gold film during femtosecond laser pulse heating. The laser pulse duration is 0.1 ps and the laser intensity is 500 J m$^{-2}$. The temperature profiles predicted from the PTS model and the conventional POS model are distinctly different. The absorbed radiation energy calculated from the POS model is confined mostly within the radiation penetration depth during the laser pulse, while the PTS model predicts a much larger heated region. As a consequence, the peak lattice-temperature rise predicted from the PTS model is much smaller than that from the conventional POT model. These differences could be very important in processes in which the temperature and the size of heated area need to be precisely controlled, such as laser micro-fabrication. The temporal lattice-temperature responses predicted from these two models are also very different. The temperature predicted from the conventional model begins to fall near the end of the laser pulse. On the other hand, the lattice temperature predicted from the PTS model is still increasing at this instant, because the microscopic electron–lattice interactions delay the lattice response to the heating pulse.

The peak electron-temperature rise is one order of magnitude larger than the peak lattice-temperature rise, and electrons and lattice are strongly out of thermal equilibrium with each other. The PTS model and the conventional model also predict totally different speeds of energy propagation. In the PTS model, electrons transfer energy and their thermal diffusivity is $\alpha_e = \kappa/C_e$. On the other hand, in the POS model, electrons are in thermal equilibrium with the lattice, which results in a much smaller thermal diffusivity, $\alpha_{eq} = \kappa/(C_e + C_\ell)$. The $\alpha_{eq}$ is typically two orders of magnitude smaller than $\alpha_e$. As a result, the PTS model predicts a much more rapid energy transport and a much larger heat-affected region than the conventional POS model.

Figure 6 presents the temperature profiles in a gold–chromium two-layer film during a 0.1 ps laser pulse heating. The POS model predicts a weak effect of the chromium underlying layer on the laser heating process, but the PTS model shows a significant effect of the chromium layer on both the electron temperature and the lattice temperature responses in the top gold layer. In the POS model, the laser energy is deposited directly into the gold lattice and then the absorbed energy propagates slowly in the lattice. Since the thermal diffusivity of gold is $\alpha_{eq} = \kappa/(C_e + C_\ell) = 1.2 \times 10^{-4}$ m$^2$ s$^{-1}$ it takes about 7 ps for a heat pulse to diffuse a 300 Å distance. During the initial laser heating process, the heat pulse does not travel far enough to reach the gold–chromium interface and thus does not feel the existence of the underlying chro-

Table 1. Physical properties of gold and chromium used in simulation

| Reflectivity, $R = 0.93$† | Radiation penetration depth, $\delta = 15.3$ nm† | |
|---|---|---|
| Parameters | Gold | Chromium |
| Initial temperature ($T_0$) | 300 K | 300 K |
| Thermal conductivity ($\kappa$) | 315 W m$^{-1}$ K$^{-1}$‡ | 94 W m$^{-1}$ K$^{-1}$‡ |
| Lattice heat capacity ($C_l$) | $2.5 \times 10^6$ J m$^{-3}$ K$^{-1}$‡ | $3.3 \times 10^6$ J m$^{-3}$ K$^{-1}$‡ |
| Electron heat capacity ($C_{e^0}$) | $2.1 \times 10^4$ J m$^{-3}$ K$^{-1}$§ | $5.8 \times 10^4$ J m$^{-3}$ K$^{-1}$§ |
| Electron–phonon coupling factor ($G$) | $2.6 \times 10^{16}$ W m$^{-3}$ K$^{-1}$¶ | $42 \times 10^{16}$ W m$^{-3}$ K$^{-1}$¶ |

† Typical value for visible light, see ‡.
‡ *American Institute of Physics Handbook* (3rd Edn). McGraw-Hill, New York (1972).
§ Ref. [28].
¶ Ref. [21].

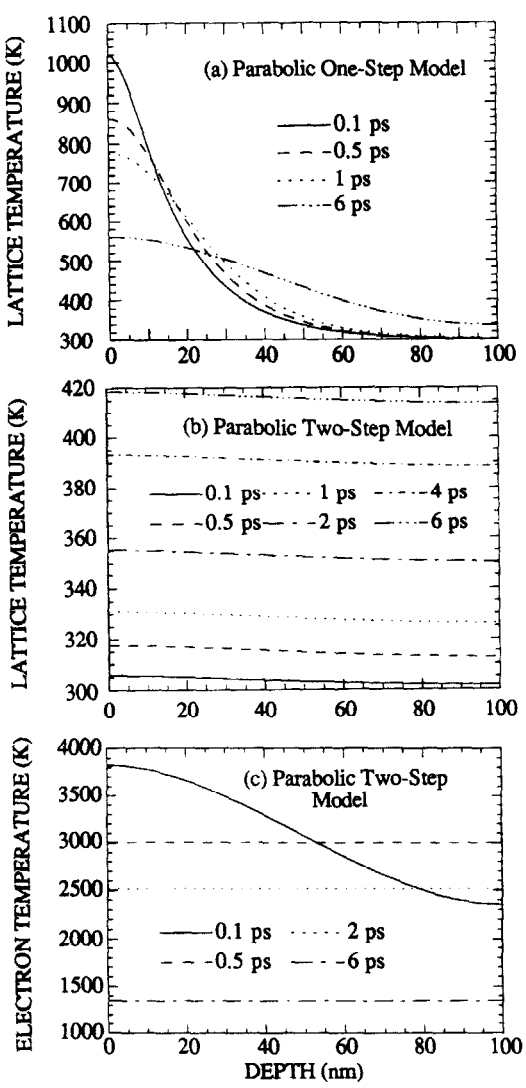


FIG. 5. Temperature profiles in a 1000 Å thick gold film during 0.1 ps laser pulse heating ($J = 500$ J m$^{-2}$).

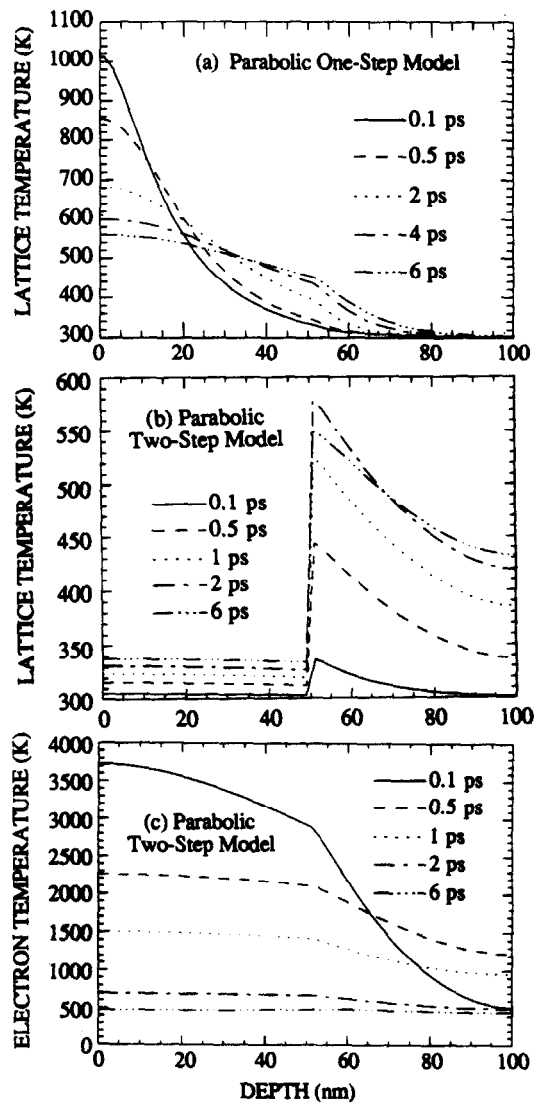


FIG. 6. Temperature profiles in a 500 Å gold/500 Å chromium two-layer film during 0.1 ps laser pulse heating ($J = 500$ J m$^{-2}$).

mium layer. After about 4 ps, the heat pulse reaches this interface. Since chromium has a lower thermal conductivity than gold, it slows down the propagation rate of the heat pulse.

In the PTS model, laser energy is absorbed by free electrons, which then undertake two simultaneous energy transfer processes: (1) electron–lattice thermalization that transfers part of the absorbed radiation energy from electrons to the local lattice; and (2) energy diffusion through random motion of electrons that carries the rest of absorbed energy away from the radiation absorption region. These two competing processes have the opposite effects on the lattice-temperature response. A stronger thermalization process results in a more localized lattice-temperature distribution and a higher lattice-temperature rise. On the other hand, a stronger energy diffusion process spreads the absorbed energy to a larger region that leads to a lower lattice-temperature rise. Due to the small heat capacity of electrons, their thermal diffusivity is very high, $\alpha_e = \kappa/C_e = 1.5 \times 10^{-2}$ m$^2$ s$^{-1}$ in gold. It takes only about 100 fs for the heat pulse to propagate across the 500 Å thick gold layer and reach the underlying chromium layer. Since chromium has a larger electron–lattice coupling factor than gold, the thermalization process in chromium is more rapid than in gold. As a result, most of the absorbed radiation energy is converted to the chromium lattice energy, although it is absorbed in the top gold layer. The lattice-temperature rise of chromium is about one order of magnitude higher than the temperature rise of the gold lattice.

Figure 7 shows transient temperature profiles in a gold–chromium–gold triple-layer film during 0.1 ps laser pulse heating. For the POS model, the structure change has negligible effects on the heating process. Introducing the sandwiched chromium layer neither increases or decreases the peak surface temperature rise. The sandwich structure has, however, very strong effects in the PTS model. The chromium layer blocks the thermal transport carried by electrons due to its low thermal diffusivity. It also converts most of the absorbed radiation energy to the lattice energy inside the chromium layer, resulting in a sandwiched distribution of the lattice temperature.

Figure 8 presents the lattice-temperature response of the gold surface during 0.1 ps laser pulse heating of multi-layer metals. Results from the POS model and the PTS model are very different. The POS model predicts both a much higher temperature rise than the PTS model and the independence of the temperature response from the film structure. On the other hand, the temperature response depends on the film structure strongly in the PTS model. The chromium layer can reduce the lattice-temperature rise significantly. These results indicate that during short-pulse laser heating the microscopic energy deposition and transport processes must be considered. Furthermore, the thermal conductivity is no longer the unique thermal parameter determining energy transfer during short-pulse laser heating; the electron–lattice coupling factor, which characterizes the energy transfer between electrons and the lattice, becomes an important thermal parameter as well.

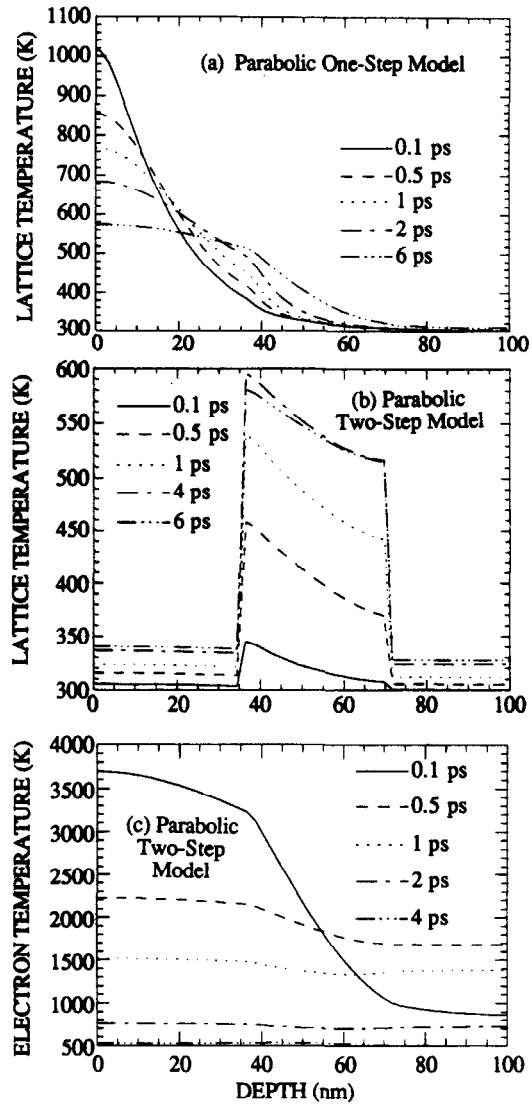


FIG. 7. Temperature profiles in a 340 Å gold/330 Å chromium/330 Å gold three-layer film during 0.1 ps laser pulse heating ($J = 500$ J m$^{-2}$).

The fact that energy deposition to the lattice does not occur where radiation energy is absorbed suggests new potential concepts for the prevention of thermal damage of mirrors in high-power laser applications. For example, the top coating layer of metal mirrors benefits from a material with both high thermal conductivity and low electron–lattice coupling to reduce the amount of lattice heating. Lattice defects in the top layer generated during coating processes should be minimized since these defects enhance the energy transfer between electrons and the lattice [18]. It might also be possible to introduce a layer of material beneath the top metal coating as an electron heat sink

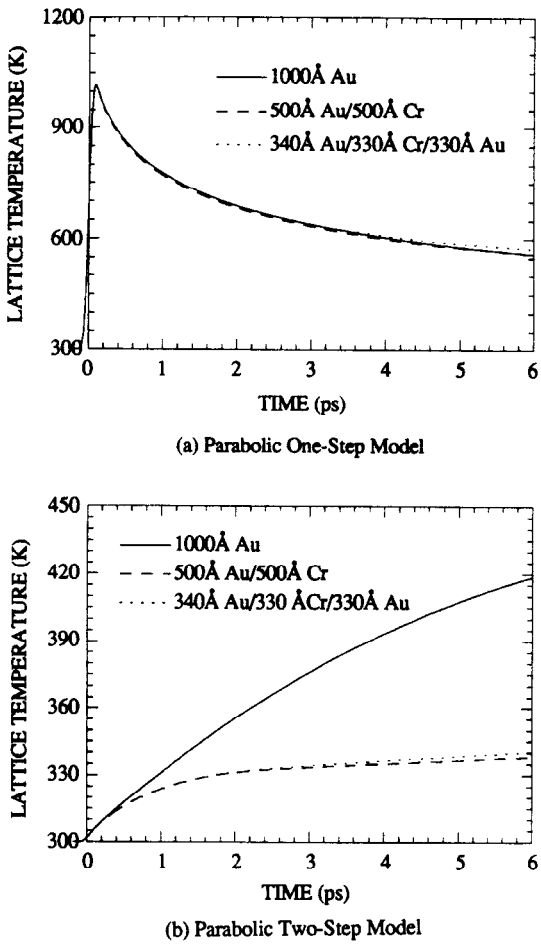


FIG. 8. Lattice-temperature responses during 0.1 ps laser pulse heating ($J = 500$ J m$^{-2}$).

that converts the absorbed radiation energy into the lattice energy in this new layer instead of in the top coating layer so that the coating layer is not overheated.

## CONCLUSIONS

This work analyses energy transfer in gold and chromium multi-layer films during femtosecond laser heating. A regime map for the applicability of different laser heating models has been constructed based on the characteristic laser heating time-scales. The microscopic radiation deposition and energy transport processes have been shown to have significant effects on the thermal response of multi-layer metals. A chromium layer beneath the top gold coating layer can significantly lower the lattice temperature rise of the gold layer. Although the laser energy is absorbed in the top gold layer, most of the absorbed energy is converted into the lattice energy at the underlying chromium layer instead of in the top gold layer. This mechanism suggests potential new design concepts for the prevention of thermal damage of mirrors in high-power laser applications.

*Acknowledgements*—The authors acknowledge the financial support from the U.S. National Science Foundation, the U.S. Department of Energy, and the K. C. Wang Education Foundation in Hong Kong.

## REFERENCES

1. S. Musikant, *Optical Materials : An Introduction to Selection and Application*. Marcel Dekker, New York (1985).
2. A. M. Prokhorov, V. I. Konov, I. Ursu and I. N. Mihailescu, *Laser Heating of Metals*. Adam Hilger, Bristol (1990).
3. A. H. Guenther and J. K. McIver, The pulsed laser damage sensitivity of optical thin films—thermal conductivity, *Laser Particle Beams* **7**, 433–441 (1989).
4. E. E. Joseph and L. Preziosi, Heat waves, *Rev. Mod. Phys.* **61**, 41–73 (1989).
5. W. S. Kim, L. G. Hector and M. N. Ozisik, Hyperbolic heat conduction due to axisymmetric continuous or pulsed surface heat sources, *J. Appl. Phys.* **68**, 5478–5485 (1990).
6. A. Kar, C. L. Chan and J. Mazumder, Comparative studies on nonlinear hyperbolic and parabolic heat conduction for various boundary conditions: analytic and numerical solutions, *J. Heat Transfer* **114**, 14–20 (1992).
7. D. Y. Tzou, Thermal shock phenomena under high rate response in solids. In *Annual Review of Heat Transfer* (Edited by C. L. Tien), Vol. IV, pp. 111–186. Hemisphere Publishing, Washington (1992).
8. L. G. Hector, W. S. Kim and M. N. Ozisik, Hyperbolic heat conduction due to a mode locked laser pulse train, *Int. J. Engng Sci.* **30**, 1731–1744 (1992).
9. R. J. von Gutfeld and A. J. Netherot, Heat pulses in quartz and sapphire at low temperatures, *Phys. Rev. Lett.* **12**, 641–644 (1964).
10. W. E. Bron, Y. B. Levinson and J. M. O'Connor, Phonon propagation by quasidiffusion, *Phys. Rev. Lett.* **49**, 209–211 (1982).
11. W. E. Bron, Phonon generation, transport and detection through electronic states in solids. In *Nonequilibrium Phonons in Nonmetallic Crystals* (Edited by W. Eisenmenger and A. A. Kaplyanskii), pp. 227–273. Elsevier (1986).
12. W. E. Bron, Phonon transport—experiment. In *Dynamical Properties of Solids* (Edited by G. K. Horton and A. A. Maradudin), pp. 1–64. Elsevier (1990).
13. T. I. Galkina, Generation and propagation of phonons in crystalline and amorphous silicon under optical excitation. In *Physics of Phonons* (Edited by T. Paszkiewicz), pp. 410–418. Springer-Verlag, Berlin (1987).
14. M. I. Kaganov, I. M. Lifshitz and L. V. Tanatarov, Relaxation between electrons and crystalline lattices, *Sov. Phys. JETP* **4**, 173–178 (1957).
15. S. I. Anisimov, B. L. Kapeliovich and T. L. Perel'man, Electron emission from metal surfaces exposed to ultrashort laser pulses, *Sov. Phys. JETP* **39**, 375–377 (1974).
16. G. L. Eesley, Observation of nonequilibrium electron heating in copper, *Phys. Rev. Lett.* **51**, 2140–2143 (1983).
17. S. D. Brorson, J. G. Fujimoto and E. P. Ippen, Femtosecond electronic heat-transfer dynamics in thin gold film, *Phys. Rev. Lett.* **59**, 1062–1965 (1987).
18. H. E. Elsayed-Ali, T. Juhasz, G. O. Smith and W. E. Bron, Femtosecond thermoreflectivity and thermotransmissivity of polycrystalline and single-crystalline gold films, *Phys. Rev. B* **43**, 4488–4491 (1991).
19. T. Juhasz, H. E. Elsayed-Ali, X. H. Hu and W. E. Bron, Time-resolved thermoreflectivity of thin gold films and its dependence on the ambient temperature, *Phys. Rev. B* **45**, 13 819–13 822 (1992).
20. H. E. Elsayed-Ali and T. Jushasz, Femtosecond time-resolved thermomodulation of thin gold films with

different crystal structures, *Phys. Rev. B* **47,** 13 599–13 610 (1993).
21. T. Q. Qiu and C. L. Tien, Short-pulse laser heating on metals, *Int. J. Heat Mass Transfer* **35,** 719–726 (1992).
22. M. J. Maurer, Relaxation model for heat conduction in metals, *J. Appl. Phys.* **40,** 5123–5130 (1969).
23. W. S. Fann, R. Storz, H. W. K. Tom and J. Bokor, Direct measurement of nonequilibrium electron-energy distributions in sub-picosecond laser-heated gold films, *Phys. Rev. Lett.* **68,** 2834–2837 (1992).
24. W. S. Fann, R. Storz, H. W. K. Tom and J. Boker, Electron thermalization in gold, *Phys. Rev. B* **46,** 13 592–13 595 (1992).
25. T. Q. Qiu and C. L. Tien, Heat transfer mechanisms during short-pulse laser heating of metals, *J. Heat Transfer* **115,** 835–841 (1994).
26. S. D. Brorson, A. Kazeroonian, J. S. Moodera, D. W. Face, T. K. Cheng, E. P. Ippen, M. S. Dresselhaus and G. Dresselhaus, Femtosecond room-temperature measurement of the electron-phonon coupling constant $\lambda$ in metallic superconductors, *Phys. Rev. Lett.* **64,** 2172–2175 (1990).
27. R. H. M. Groeneveld, Femtosecond spectroscopy on electrons and phonons in noble metals, Ph.D. thesis, Van der Waals—Zeeman Laboratory, University of Amsterdam (1992).
28. C. Kittel, *Introduction to Solid State Physics* (6th Edn). Wiley, New York (1986).
29. R. W. Powell and C. Y. Ho, The state of knowledge regarding the thermal conductivity of the metallic elements. In *Thermal Conductivity* (Edited by D. R. Flynn and B. A. Peary. Jr.), pp. 1–31. National Bureau of Standards, Gaithersburg, MD (1967).
30. W. J. Scouler, Temperature-modulated reflectance of gold from 2 to 10 eV, *Phys. Rev. Lett.* **18,** 445–448 (1967).
31. G. P. Pells and M. Shiga, The optical properties of copper and gold as a function of temperature, *J. Phys. C* **2,** 1835–1846 (1969).